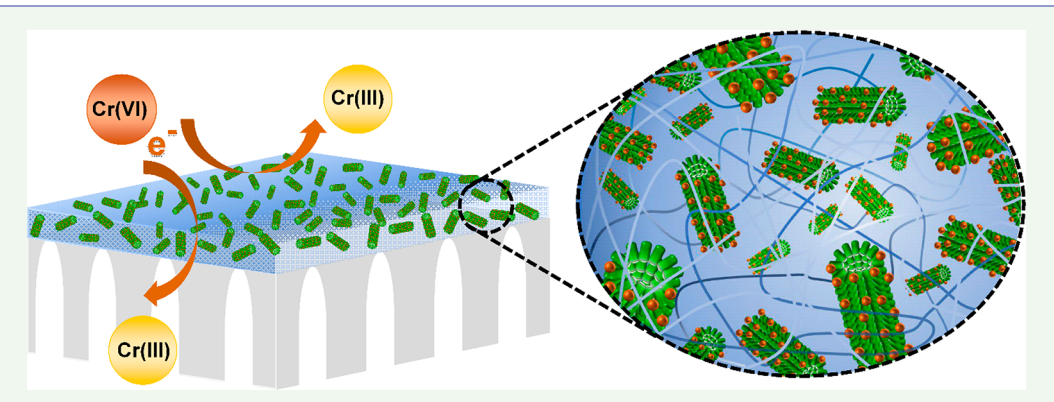
# Membranes with Thin Hydrogel Selective Layers Containing Viral-Templated Palladium Nanoparticles for the Catalytic Reduction of Cr(VI) to Cr(III)

Ilin Sadeghi, Eric Y. Liu, Hyunmin Yi,\* and Ayse Asatekin\*

Chemical and Biological Engineering Department, Tufts University, Medford, Massachusetts 02155, United States

Supporting Information



ABSTRACT: Membranes that simultaneously remove large organic molecules and catalytically treat smaller contaminants can provide a simple, compact, single-step water treatment solution. Incorporating nanoparticles (NPs) into membranes can impart catalytic activity but is extremely challenging to achieve while preventing aggregation, maintaining high stability, and retaining accessibility to the NP surfaces. Here, we present a new tunable and scalable strategy, interfacially initiated free radical polymerization (IIFRP), for hybrid water filtration membranes incorporating small, uniform, well-dispersed catalytic NPs immobilized on tobacco mosaic virus (TMV) nanotemplates within their ultrathin hydrogel selective layers. Hybrid membranes are prepared by adding the TMV-templated NPs to the monomer solution during IIFRP. These membranes catalytically reduce Cr(VI), an acutely toxic and carcinogenic contaminant, to Cr(III), an essential nutrient. The catalytic NPs are fully accessible to the reactants within the hydrogel and exhibit extremely high catalytic activity, achieving up to 98% conversion in a single pass. Furthermore, because of the hydrogel network, these NPs are exceptionally stable, fully retaining their catalytic activity with continuous filtration for at least 3 days. These results illustrate a versatile approach for integration of various nanomaterials within membrane selective layers, enabling the creation of advanced membranes with new and versatile functionalities for nextgeneration applications.

KEYWORDS: catalytic membrane, hydrogel, ultrathin, hybrid membrane, biotemplated nanomaterials

# ■ INTRODUCTION

Hexavalent chromium, Cr(VI), is the third most common pollutant in hazardous waste sites and the second most common inorganic contaminant after lead. Its widespread industrial applications (e.g., corrosion control, leather tanning, pigment manufacturing, photography, and electroplating) and its ubiquity in nature have made it a prolonged environmental concern.<sup>2,3</sup> The World Health Organization (WHO) has strictly regulated Cr(VI) levels below 50 ppb for safe drinking water.4 This acute toxicity has long attracted extensive research for environmental remediation of Cr(VI), resulting in the development of various remediation methods such as precipitation, ion exchange, electrochemical treatment, and adsorption. 5,6 However, these conventional methods are still plagued with several limitations such as low efficiency, high energy requirements, and large amount of toxic waste sludge.

Thus, developing a simple and efficient method for the treatment of this toxic compound that is released in large quantities still remains a challenge. While Cr(VI) is acutely toxic, mutagenic, and carcinogenic, its reduced state, Cr(III), is considered a trace element needed in human diet.8 Hence, reductive transformation of Cr(VI) to Cr(III) presents a promising approach to remediate water streams contaminated with Cr(VI).

Another major challenge in water treatment is the simultaneous remediation of pollutants whose sizes differ by several orders of magnitude, such as particulates and diseasecausing bacteria (micrometers), along with addressing Cr(VI)

Received: June 7, 2019 Accepted: July 31, 2019 Published: July 31, 2019



ions (<1 nm). Membrane processes that combine catalytic reduction capability with size-sieving filtration can potentially accomplish this in a single, simple, energy-efficient, and easy to operate unit.9,10 Catalytic membranes operate at lower pressures than filters that would retain heavy metal ions, such as reverse osmosis (RO) and nanofiltration (NF) membranes. They also do not create a concentrated Cr(VI) waste that needs to be managed after removal, unlike RO/NF membranes or adsorption systems. Unlike common catalytic reactors packed with porous catalytic particles, convective flow through the catalytic membrane facilitates enhanced contact between the reactants and catalyst surface, circumventing mass transfer limitations that arise from slow diffusive transport of solutes to the catalyst sites. The continuous removal of products results in less accumulation, competition, and side reactions on the catalyst's active sites. This not only alleviates catalyst poisoning<sup>11,12</sup> but also decreases possible product inhibition and enhances overall reaction rates. 9,13

Metal nanoparticles (NPs) are of great interest due to their superior catalytic activity as a result of high surface area-tovolume ratios. 14 Palladium (Pd) NPs are well-known for their high catalytic activity toward the reduction of Cr(VI) to Cr(III)<sup>15-17</sup> as well as other important catalytic conversions. 18-20 However, the critical problem has long been developing an efficient, simple, and scalable approach for integrating NPs within the membrane that provides stability to otherwise highly aggregate-prone NPs. Several methods have been reported for incorporating catalytic NPs in membranes, including physical blending of NPs in the casting solution,<sup>21</sup> adsorption of metal precursor by anchoring to polymer functional groups followed by in situ reduction to form NPs, 17,20,24,25 using an adhesive polymer layer such as polydopamine to attach NPs on the membrane surface, 26 and layer by layer assembly by sequential deposition of polyelectrolytes and NPs on commercial support membranes.<sup>28–30'</sup> However, complex structure and chemistries, as well as difficult, lengthy, and/or harsh fabrication conditions, make these approaches challenging for large scale manufacturing and utilization. More importantly, these approaches still suffer from inherent limitations that can severely restrict their applicability. First, immobilizing sufficient quantities of NPs into the membrane to reach high conversions is challenging. Second, it is difficult to form uniform and well-dispersed NPs within the porous structure of the membrane, which, when successful, provides catalyst surface area that can be orders of magnitude higher than membrane surface area alone. 26,27 Moreover, stability (i.e., retention of the catalytic activity) for continuous operation still remains a critical issue. Finally, integrating nanomaterials using most of these methods will either entrap them within the bulk membrane matrix, severely limiting their accessibility to the reactants,<sup>31</sup> or leave the NPs exposed to feed and other contaminants. This not only increases the risk of leaching<sup>28</sup> and agglomeration<sup>26,32</sup> but also results in fouling and catalyst poisoning, <sup>33</sup> especially when used in wastewater treatment. <sup>11,34</sup> Some of this can be managed by frequent regeneration, but a slow, irreversible decline in catalytic activity occurs nonetheless. 32,33 The development of catalytic membranes with longer term stability would thus enable the continuous remediation of larger quantities of toxic waste with less downtime for regeneration and recovery.

Viral nanomaterials are particularly attractive as nanoscale templates for controlled synthesis of very small, stable, and uniform metal NPs. This arises from their well-defined

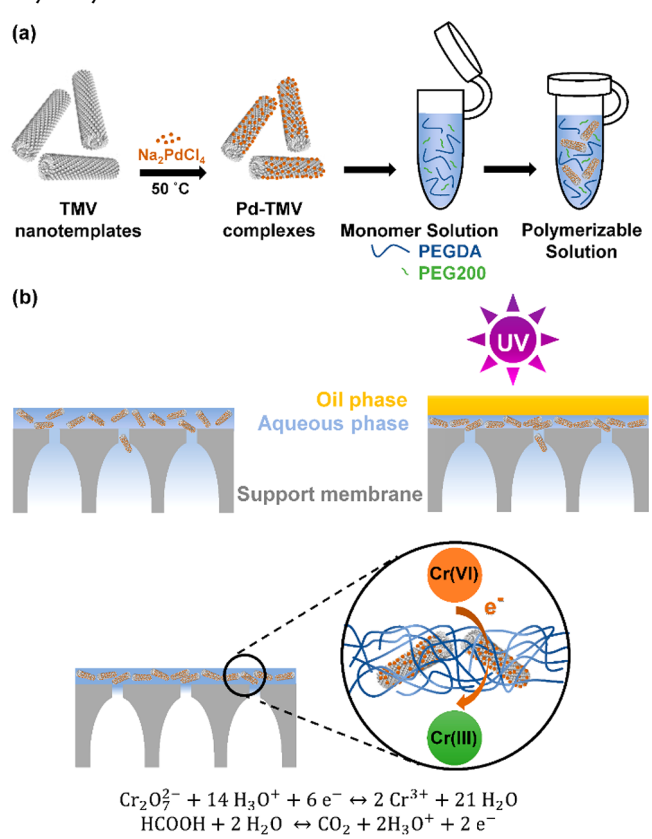
structure, monodisperse nature, abundant surface functionalities, and stability in various solvents. The tobacco mosaic virus (TMV) exhibits these features exquisitely. Its tubular structure with precise dimensions (18 nm diameter × 300 nm, hydrodynamic diameter  $(D_h) \sim 110 \text{ nm}$ , 35 stability in a wide range of conditions (e.g., pH 2-10, temperature up to 90 °C), biological safety, and ease of mass production make TMV a potent nanotemplate.<sup>36</sup> In addition, genetically displayed cysteines on TMV (e.g., TMV1cys) can significantly enhance Pd NP formation because of improved biosorption of the precursors.<sup>37</sup> A simple synthesis approach using TMV as nanotemplates in mild aqueous conditions thus provides an attractive route for the controlled synthesis of small (1–2 nm), uniform, and well-dispersed Pd NPs with high catalytic activity.<sup>38</sup> Seamless integration of these nano-biocomplexes into a robust platform that provides long-term stability for these NPs within the matrix and easy access of the reactants is required to achieve high conversion during continuous filtration.

Hydrogels are excellent stabilizing platforms for viral or metal NPs due to their high stability and three-dimensional (3D) microporous structures, providing improved accessibility and ready diffusion of reactants to active NPs.<sup>38</sup> They are also very promising materials in membrane applications because they are versatile, easily tunable, and functionalizable.<sup>3</sup> Hydrogels are typically incorporated into membranes by forming a thin layer on top of a porous support layer with better mechanical properties. If the hydrogel layer is continuous and the support layer has relatively large pores, the hydrogel layer acts as a selective layer that controls membrane selectivity through its mesh size. The inherently hydrophilic nature and high fouling resistance of hydrogels 40,41 make them especially suitable for wastewater treatment, where fouling is a critical concern. <sup>42–45</sup> In particular, poly(ethylene glycol) (PEG)-based hydrogels are inexpensive and environmentally friendly<sup>46</sup> and have been reported as both reducer and stabilizer for the synthesis of Pd NPs in several reactions. 18,47-49 Hence, integrating the NPs within a PEGDA network could lead to hybrid hydrogels with potent synergistic properties. 50,51 We therefore expect that the encapsulation of catalytic NPs in hydrogel membrane selective layers can prevent the access of foulants or macromolecules that might be present in wastewater, thus preserving catalytic functionality. 39,52,53 To fabricate these catalytically active hydrogel selective layers with multiple functionalities, a simple and scalable method is required that will enable seamless integration of catalytic NPs within the hydrogel membrane selective layer. The resultant membrane architecture should also provide long-term stability and minimal leaching of these NPs for continuous operation under applied pressure. Finally, the manufacturing method should enable fine control over metal NP loading. Such a method could significantly broaden the application of hydrogels for environmental remediation.

Here, we describe a novel approach for fabricating membranes with catalytically active hydrogel selective layers and demonstrate its capabilities in the context of catalytic reduction of Cr(VI) during filtration. This work builds on our recently developed technique, interfacially initiated free radical polymerization (IIFRP), which enables fabrication of ultrathin hydrogel selective layers on porous supports. To create multifunctional membranes that catalytically reduce pollutants, we expanded this technique to seamlessly integrate virus-supported catalytic NPs into hydrogel selective layers and

create hybrid membranes (Scheme 1). To achieve this, we first prepared uniform Pd NPs on TMV1cys nanotemplates

Scheme 1. Schematic Showing the Method Used for the Preparation of Catalytic Membranes Containing TMV-Templated Pd Nanoparticles Using IIFRP: (a) Formation of Monomer Solution Containing Pd-TMV Complexes; (b) Formation of the Pd-TMV-Containing Hydrogel Selective Layer by IIFRP



(Scheme 1a). These Pd-TMV complexes were then integrated into hydrogel membrane selective layers via IIFRP (Scheme 1b). As illustrated in Scheme 1, the aqueous monomer solution containing monomer, porogen, and Pd-TMV complexes is first poured on a support membrane. Monomer solution fills the membrane's large pores and leaves a thin top layer on the membrane surface. The catalytic Pd-TMV complexes mostly remain on the membrane surface due to their large size. A hydrophobic oil layer containing photoinitiator (PI, Darocur 1173) is then added to cover the membrane surface. Upon UV irradiation, polymerization starts at the interface spanning the surface of the support membrane. This creates a uniform and ultrathin hydrogel selective layer in which Pd-TMV complexes are embedded, imparting high catalytic activity in a simple and controlled manner. These membranes exhibited extremely high catalytic activity for the reduction of Cr(VI), achieving up to 98% conversion in single pass filtration experiments. The catalytic property remained highly stable during continuous long-term operations for at least 3 days. Furthermore, detailed reaction kinetics studies showed a strong correlation between the Pd loading in the monomer solution and membranes' catalytic activity, suggesting ease of control over NP loading by IIFRP. Taken together, these results illustrate a versatile method for controlled fabrication of robust,

catalytically active hydrogel selective layers in a simple, reproducible, and scalable manner. We envision that the method utilized here can be readily expanded for fabrication of multifunctional membranes toward a wide range of applications and complex waste streams.<sup>54</sup>

# RESULTS AND DISCUSSION

Spontaneous Formation of Pd Nanoparticles on TMV Nanotemplates. The first step in the formation of the catalytic membranes involves the preparation of palladium (Pd) nanoparticles (NPs) templated and immobilized on tobacco mosaic virus (TMV) genetically modified with cysteines (TMV1cys)<sup>37</sup> (Scheme 1a). We first synthesized small and uniform Pd NPs along these TMV nanotemplates (Figure 1). For this, a solution of 10 mM Na<sub>2</sub>PdCl<sub>4</sub> was mixed

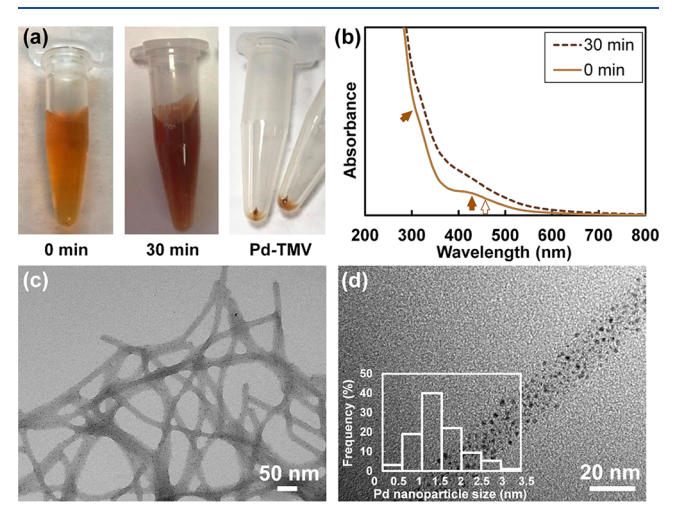


**Figure 1.** Formation and characterization of Pd–TMV complexes. (a) Photographs of Pd–TMV solution before incubation (left) and after incubation at 50 °C (middle) and Pd–TMV pellets after centrifugation (right). (b) UV–vis absorbance of Pd–TMV solution before and after incubation. Solid arrows indicate absorption peaks associated with PdCl $_3$ , whereas the hollow arrow shows the absorption peak due to PdCl $_4$  $^2$ - ions. (c) TEM images of spontaneously formed Pd NPs along TMV biotemplates. (d) Higher magnification of (c) showing the histogram of Pd NP size.

with 0.6 mg mL<sup>-1</sup> TMV1cys and incubated at 50 °C for 30 min, as in our recent report.<sup>38</sup> Macroscopic images of the reaction mixture at the beginning and end of the incubation are shown in Figure 1a. The color changed from yellow-brown to dark brown upon 30 min of incubation, suggesting the formation of Pd-TMV complexes that can be readily separated with centrifugation. The formation of Pd-TMV complexes is also confirmed by the UV-vis absorbance spectra (Figure 1b), consistent with our recent report.<sup>38</sup> Before incubation, Pd is predominantly in the form of PdCl<sub>3</sub>(H<sub>2</sub>O)<sup>-</sup> and PdCl<sub>4</sub><sup>2-</sup> ions, as evidenced by the characteristic absorbance peaks for these species. A strong peak around 430 nm and a small shoulder at 320 nm correspond to PdCl<sub>3</sub>(H<sub>2</sub>O)<sup>-</sup>(marked with solid arrows in Figure 1b). Strong absorbance below 300 nm and a small shoulder peak at about 475 nm are indicative of PdCl<sub>4</sub><sup>2-</sup> ions (marked with a hollow arrow in Figure 1b).<sup>55</sup> Upon 30 min incubation, these peaks are replaced by increased absorbance over a broad wavelength range correlated to rapid conversion of Pd precursors to Pd-TMV complexes.

ACS Applied Nano Materials Article

Table 1. Aqueous Monomer Solution Compositions and Permeances of the Prepared Membranes

	monomer solution content				
membrane code	PEGDA ( % v/v)	PEG200 (% v/v)	TMV (mg mL <sup>-1</sup> )	Pd <sup>a</sup> (mg mL <sup>-1</sup> )	permeance (L $m^{-2} h^{-1} bar^{-1}$ )
M0	5	2.5	0	0	$3.3 \pm 0.5$
M1	5	2.5	1	1.7	$9.6 \pm 0.8$
M3	5	2.5	3	5.3	$4.2 \pm 0.6$
M10	5	2.5	10	17.5	$2.1 \pm 0.1$
<sup>a</sup> Assuming complete conversion of the Pd precursor to NPs.					

(a) (b) (c) Hydrogel layer  $_{\gamma}$  120 nm 100 nm 200 nm

Figure 2. Morphology of a hybrid hydrogel selective layer formed by IIFRP. (a) SEM image of the membrane surface. (b) AFM micrograph showing the membrane surface. (c) Membrane cross section. The inset shows higher magnification of the selective layer. The scale bar in the inset is 200 nm.

Next, we examined the structure and distribution of Pd NPs along TMV nanotemplates via TEM (Figure 1c,d). For this, the Pd-TMV solution was centrifuged at 9000g for 5 min after incubation. Then, Pd-TMV pellets were collected and suspended in deionized (DI) water before being placed on a TEM grid. Figure 1c shows the formation of interlocking networks of Pd-TMV, stemming from the screening of the repulsive forces between negatively charged amino acids on the TMV-coated proteins by Pd precursors.<sup>56</sup> No Pd aggregates outside the TMV nanotemplates were observed, confirming preferential precursor adsorption and Pd NP growth exclusively on TMV templates, consistent with our recent study.<sup>38</sup> A higher magnification image (Figure 1d) illustrates small and well-dispersed Pd particles on the TMV nanotemplates more clearly. The histogram of Pd NP sizes, shown in the inset of Figure 1d, also reflects the narrow size distribution with an average size of 1.7  $\pm$  0.3 nm (calculated based on 100 particles). The high-resolution TEM image of Pd NPs on the TMV biotemplates (Figure S1, Supporting Information) further confirms the small size of the Pd NPs as well as their highly crystalline structure.

Overall, the results in Figure 1 confirm that well-dispersed and small Pd NPs form spontaneously and exclusively on the TMV simply by mixing Na<sub>2</sub>PdCl<sub>4</sub> and TMV solution in mild aqueous conditions, clearly demonstrating the utility of TMV as nanotemplates. <sup>38,57</sup> Importantly, TMV's robust, rod-shaped structure provides a stable scaffold to keep the Pd NPs well-dispersed without aggregation. Such good dispersion is important for catalytic and membrane applications for high surface area-to-Pd mass ratio, enhanced contact with reactants, and long-term stability.

Fabrication of Hybrid Hydrogel Selective Layers Containing Pd–TMV Nanocomplexes by IIFRP. Once the Pd–TMV complexes were prepared, we aimed to integrate them into ultrathin hydrogel membrane selective layers by using our recently developed technique, interfacially initiated free radical polymerization (IIFRP).<sup>41</sup> For this purpose, as shown in Scheme 1b, we first prepared an aqueous monomer solution containing a mixture of the Pd–TMV complexes along with the hydrophilic monomer, poly(ethylene glycol) diacrylate (PEGDA, average  $M_n = 700 \text{ g mol}^{-1}$ ). We also

added a porogen, poly(ethylene glycol) (PEG 200, average  $M_n$ = 200 g mol<sup>-1</sup>), which was shown to act as an inert additive that improves membrane flux without negatively impacting selectivity. 41 Concentrations of PEGDA and PEG 200 in the aqueous solution were kept constant at 5% and 2.5% v/v, respectively, while the Pd-TMV concentration was varied (Table 1). We poured this aqueous solution on a commercial polysulfone ultrafiltration membrane (PS35, 20 kDa, Nanostone), used as the porous support. Next, we removed the excess solution and covered the membrane surface with a hydrophobic oil layer, n-hexadecane, containing 0.1% v/v of the hydrophobic photoinitiator (PI), Darocur 1173. We then fabricated the hydrogel selective layer by exposing the support membrane to UV light using a hand-held lamp. The UV irradiation causes the PI to dissociate in the oil phase and diffuse to the oil/water interface, which initiates the free radical polymerization of PEGDA. To prevent the initiation of polymerization from the PS support membrane surface upon exposure to certain wavelengths of UV light, the membrane surface was covered with a glass plate.<sup>58</sup>

The morphology of the membranes was characterized using FESEM and AFM (Figure 2 and Figure S2). The surface FESEM and AFM images of membranes with the highest TMV concentration, M10 (Figure 2a,b), show that the Pd-TMV complexes are successfully embedded in the hydrogel layer. They also illustrate individual, nonaggregated Pd-TMV complexes well-dispersed throughout the hydrogel layer over the entire membrane, imaged in different frames sampling length of the sample (data not shown). Similar well-distributed Pd-TMV complexes were obtained for all Pd-TMV concentrations without any apparent aggregation (Figure S2). All hybrid membranes showed similar RMS surface roughness values (Table S1), but much rougher surfaces compared to the hydrogel-coated membrane without any Pd-TMV (M0), further confirming the incorporation of the Pd-TMV complexes into the selective layer. The cross-sectional SEM image of the hydrogel membrane (Figure 2c) shows the formation of an ultrathin layer with dry thickness of about 120 nm on the support membrane (Figure S3). The higher magnification image in the inset depicts the uniform nature of the hydrogel layer throughout its thickness. It also clearly

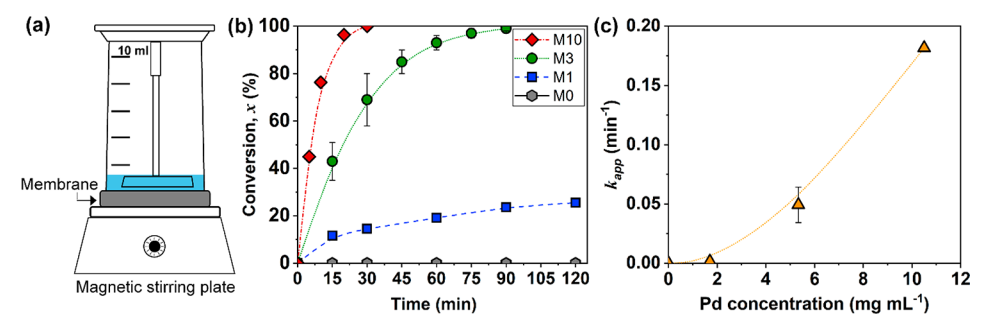


Figure 3. Catalytic activity of membranes in batch experiments. (a) Schematic of the experimental setup used to conduct static reactions. (b) Conversion of dichromate catalyzed by hybrid membranes with different loading densities. (c) Apparent rate constant vs Pd loading densities in monomer solution, calculated assuming complete conversion of Pd precursor to Pd NPs.

illustrates the integration of the Pd-TMV complexes into the selective layer without any observable defects. Combined, the results in Figure 2 demonstrate that IIFRP provides a simple, robust, and scalable approach for integration of Pd-TMV complexes into hydrogel selective layers.

Membrane Performance: Pure Water Permeance. To study the permeance of these membranes and the effect of different Pd-TMV loadings, we performed filtration experiments using a dead-end setup (Table 1). For this, DI water was filtered through the membranes prepared as described in the previous section until a stable flow rate was obtained. Pure water permeance, defined as water flux through the membrane normalized by the applied transmembrane pressure of 2.7 bar (40 psi), was then calculated. The support membrane permeance was measured to be  $1250 \pm 60 \text{ L h}^{-1} \text{ m}^{-2} \text{ bar}^{-1}$ . Table 1 shows the water permeances of these Pd-TMV hydrogel-coated membranes. The hydrogel-coated membrane containing no Pd-TMV particles shows a permeance of 3.3 ± 0.5 L h<sup>-1</sup> m<sup>-2</sup> bar<sup>-1</sup> (first row). The addition of even a small amount of Pd-TMV complexes led to an increase in permeance to 10 L h<sup>-1</sup> m<sup>-2</sup> bar<sup>-1</sup>. However, as more Pd-TMV was loaded, the permeance decreased to 2.0 L h<sup>-1</sup> m<sup>-2</sup> bar<sup>-1</sup> for the hydrogel with the highest Pd-TMV content examined, M10. As the amount of Pd-TMV increased in the hydrogel selective layer, the volume fraction of the layer that allows water passage decreased. 59-61 All hydrogel layers containing Pd-TMV complexes showed industrially relevant water permeance values.6

Catalytic Activity of Hybrid Hydrogel Membranes. Batch Catalysis Experiments. We next examined the catalytic activity of these membranes in batch reactions for the reduction of Cr(VI) to Cr(III) in the presence of formic acid as the electron donor/reducing agent 63,64 (Figure 3). As discussed in more detail below, these initial analyses were performed in the presence of an excess of formic acid to better characterize reaction kinetics and to investigate the catalytic activity of these membranes in ideal conditions. They were also performed by using relatively concentrated dichromate solutions (0.1 mM K<sub>2</sub>Cr<sub>2</sub>O<sub>7</sub>, corresponding to ~10.4 mg/L Cr(VI) ions) so that even high conversions can be measured accurately. We should point out that these concentrations are over an order of magnitude higher than even highly contaminated groundwater streams. For instance, the concentration of Cr(VI) in groundwater at sites contaminated by Pacific Gas & Energy (PG&E) plants were reported to be 300–580  $\mu$ g/L in two different publications. <sup>65,66</sup> However, given the well-documented reaction kinetics for the catalytic NPs used in this study, 38,63,67 provided there is sufficient

reducing agent and negligible mass transfer limitations, percent conversion values measured in this study should be independent of feed concentration.

In these experiments, 1 mL of the reaction solution containing 0.1 mM potassium dichromate ( $K_2Cr_2O_7$ ) and 100 mM sodium formate (NaCOOH) at pH 3 were added on top of a 1 in. diameter hybrid membrane swatch held by an Oring in a stirred cell (Figure 3a).<sup>68</sup> The solution was stirred at about 200 rpm with a magnetic stirrer suspended slightly above the membrane. Membranes prepared with various amounts of Pd–TMV in the aqueous monomer solution (listed in Table 1) were tested, and the reaction was monitored at Cr(VI) ion's characteristic absorption peak at 350 nm via UV–vis spectrophotometry.

Figure 3b depicts the conversion of dichromate in the solution in contact with membranes containing various amounts of Pd-TMV. The hydrogel membrane (M0) did not show any reduction (triangles, bottom curve). The same was true for the membrane containing only TMV without Pd NPs, indicating that the TMV-containing hydrogel membrane is not catalytically active for this reaction in the absence of Pd NPs. In contrast, all hybrid membranes with Pd-TMV complexes exhibited catalytic activity to different extents, correlated to the Pd-TMV loading. The membrane with the highest Pd-TMV loading, M10 (Figure 3b, diamond, top curve), clearly showed the highest catalytic activity, with conversion reaching completion within 30 min. M3 also showed fairly high conversion, reaching near completion in about 60 min. These results show that the embedded NPs are readily accessible to both K2Cr2O7 and HCOOH and that hybrid membranes demonstrate high catalytic activity toward Cr(VI) reduction. To confirm that the removal of Cr(VI) is due to the catalytic reduction of Cr(VI) to Cr(III) rather than adsorption on the membrane, we added excess NaOH to the reacted solution to reoxidize all Cr(III) to Cr(VI). This led to reappearance of Cr(VI)'s characteristic absorption peak via oxidation of Cr(III), 67 further confirming the catalytic reduction of Cr(VI) to Cr(III) (Figure S4).

To better characterize the catalytic activity of these membranes, we calculated the apparent rate constants and examined their relationship with Pd loading densities in monomer solution (Figure 3c). The reduction reaction follows apparent pseudo-first-order batch reaction kinetics with respect to Cr(VI) concentration under the reaction conditions enlisted here. This is evident from a linear correlation between  $\ln(1-x)$  vs reaction time, where x represents the conversion. Thus, the apparent rate constant  $k_{\rm app}$  (min<sup>-1</sup>) for membranes containing various concentrations of Pd–TMV can be

obtained from the slope of linear regression of the corresponding plot. Figure 3c shows the average  $k_{app}$  vs Pd concentration in the monomer solution. Because the conversion of Pd precursor to Pd NPs is shown to be high (>80-90%),<sup>38</sup> this value is expected to be directly proportional to the concentration of Pd NPs in the monomer solution used in manufacturing the membrane and thus with the loading of Pd NPs in the membrane selective layer. As expected, increasing the Pd-TMV loading leads to higher  $k_{app}$ values, indicating a good correlation between the Pd concentrations in the monomer solution and the apparent rate constants, consistent with our recent study.<sup>38</sup>

Formic acid was chosen as the electron donor (i.e., a reducing agent) in these initial experiments to examine catalytic properties of this system under well-understood conditions. While formic acid is not present in natural water streams, several other naturally occurring organic compounds have been shown to reduce dichromate and other metal ions. For instance, Cr(VI) is known to be reduced in contaminated soils by functional groups such as carboxylic acids, alcohols, and phenols commonly found in humic substances (humic acid, fulvic acid, and humin) or as contaminants in association with chromium (e.g., oxalate ions).<sup>69</sup> Therefore, while these initial studies utilize formic acid as a well-understood reducing agent, our conclusions can potentially be applied to more realistic systems, where formic acid is replaced by these naturally occurring compounds. Alternatively, if this is the desired treatment approach, formic acid can be added to the feed to the proposed membranes to improve remediation.<sup>70</sup>

In sum, the batch catalytic reaction results in Figure 3 clearly demonstrate the catalytic activity of the hybrid membranes and robustness of our integrated synthesis-fabrication method with the ability to impart controlled catalyst loading by tuning simple fabrication parameters.

Flow-Through Mode: Dead-End Filtration. While the experiments described above show that these membranes can potentially be used for Cr(VI) reduction, they do not demonstrate the conditions under which these membranes would be used. Pressure-driven flow through the membrane would change mass transfer effects that control the access of reactants to the catalytic NPs and the removal of products. To determine the efficiency of these hybrid membranes for the reduction of Cr(VI) under flow conditions, we performed filtration experiments in which we monitored the concentration of Cr(VI) in the permeate over time (Figure 4). For this, the reaction solution containing Cr(VI) was filtered through the membrane at transmembrane pressure (TMP) of

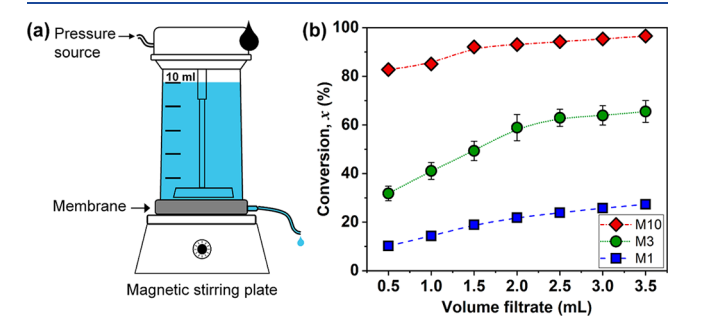


Figure 4. Catalytic activity of membranes in single-pass, dead-end filtration experiments. (a) Schematic of dead-end filtration system. (b) Conversion of Cr(VI) vs total volume of permeate collected.

1 bar in a 10 mL dead-end stirred filtration cell (Figure 4a). Filtrate fractions (0.5 mL) were continuously collected, and conversion was calculated by measuring the Cr(VI) concentration in them via UV-vis spectrophotometry. The experiment was conducted using each of the three hybrid membranes tested in batch experiments (Figure 3).

Figure 4b shows the conversion of Cr(VI) versus the total volume of filtrate collected for each of these membranes. Higher Cr(VI) reduction was achieved at higher Pd-TMV loading. The membrane containing the largest amount of Pd-TMV complexes (M10, diamond) showed near-complete conversion (>96%) in a single pass. As expected, lower Pd-TMV loading resulted in lower conversion, but still fairly high conversions of about 70% and 30% was achieved for M3 and M1, respectively. For all hybrid membranes, conversion slowly increased with time due to the configuration of the filtration setup (Figure 4a). The feed solution in the stirred cell is exposed to the catalytic NPs on the membrane surface throughout the filtration experiment. This leads to some degree of conversion in the retentate. Indeed, for all hybrid membranes, a similar conversion of about 34  $\pm$  4% was obtained for the retentate solution at the end of the experiment. Nonetheless, even early stage conversions were substantially higher in the filtrate compared with the retentate. For example, the M10 membrane showed a conversion of around 82% in the beginning of the experiment. This value then increased further throughout the experiment (top curve in Figure 4b). In summary, the high conversion values demonstrate that defect-free membranes prepared by this simple and robust method can effectively treat Cr(VI)contaminated streams in single-pass filtration experiments and achieve high degree of removal without complicated additional processing steps.

Long-Term Stability of Catalyst NPs within Hydrogel Selective Layer in the Flow-Through Mode. In addition to high activity, the stability of the catalyst NPs is crucial for catalytic membranes. Aggregation of NPs after a few cycles can significantly deteriorate their catalytic activity after repeated use. If NPs are not firmly immobilized on the membranes, they can leach out, leading to a decrease in catalytic activity. Therefore, retaining high catalytic activity is crucial for membranes to ensure reliable long-term operation. We thus examined the stability of the hybrid membranes over an extended period of time (Figure 5). We also aimed to observe the effect of residence time, the time that the solution is in contact with the membrane, on conversion. At lower TMPs, a lower flux and thus a higher residence time is expected, leading to a higher conversion.

As described above, contact between the solution and the membrane surface in a stirred dead-end cell results in some extent of conversion in the feed solution. This leads to a drift in the concentration of Cr(VI) in the feed over time, which can complicate data analysis. To avoid this, we conducted these experiments using an in-line filter holder with an effective filtration area of 0.9 cm<sup>2</sup>, connected to a 4 L reservoir (Figure 5a). This allowed us to solely examine the conversion that occurs within the hydrogel selective layer. We selected the two membranes prepared with lower Pd-TMV amounts, M1 and M3, as examples. These membranes were selected as they combined catalytic activity with relatively higher permeances. The reaction mixture was continuously fed to the membrane, and samples were collected periodically by using a fraction collector. The reduction of Cr(VI) was monitored by UV-vis ACS Applied Nano Materials Article

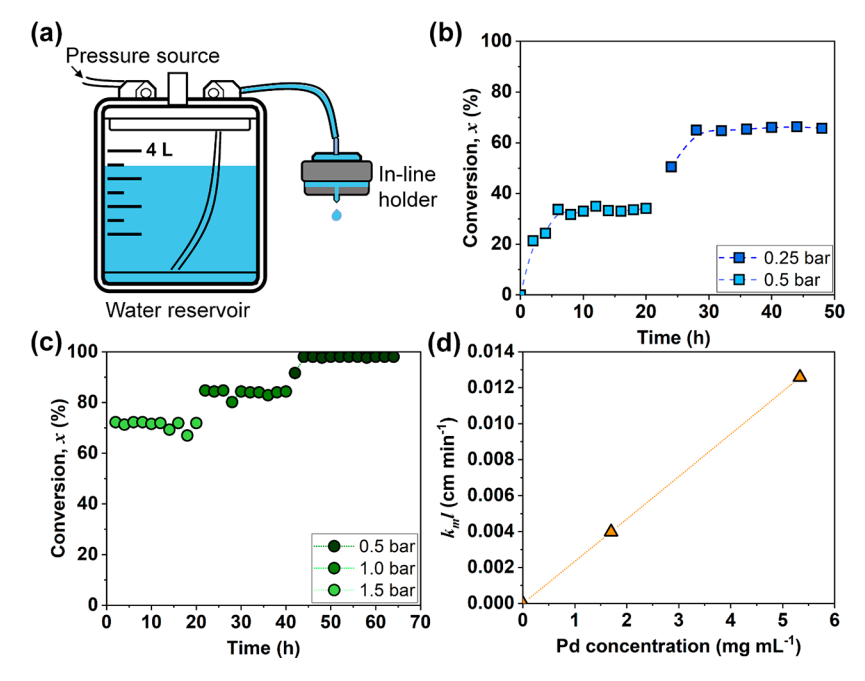


**Figure 5.** Long-term filtration experiments using an in-line filter holder and the effect of residence time on catalytic conversion of Cr(VI). (a) Schematic of continuous, in-line filtration system. (b, c) Conversion of Cr(VI) in long-term experiments at various TMP values with (b) M1 and (c) M3 membranes. (d)  $k_m l$  vs Pd concentration in the aqueous solution used in preparing the membrane.

as above. The TMP was varied during the experiment to observe the effect of residence time on conversion.

Figure 5b illustrates the conversion of Cr(VI) upon passing through the M1 membrane over 48 h, first at a TMP of 0.5 bar and then of 0.25 bar. As expected, a higher single-pass conversion was obtained at the lower TMP (top curve, Figure 5b), which corresponds to a higher residence time of Cr(VI) within the membrane selective layer. The single pass Cr(VI) conversion was 35% at a TMP of 0.5 bar when the membrane with the lowest NP loading, M1, was used (bottom curve, Figure 5b). Importantly, the membrane retained its catalytic activity for 20 h, indicating that the NPs remained highly stable within the hydrogel layer. Subsequently, the pressure was decreased to 0.25 bar. This led to a significant increase in conversion to about 65%, about twice the value obtained at 0.5 bar. Similarly, no decline in conversion was observed during the next 24 h of continuous operation. This clearly confirms that the integrity of NPs is retained with no sign of catalytic poisoning or catalyst leaching upon extended exposure to reaction solution.

A similar experiment was performed with the hybrid membrane containing a higher Pd-TMV loading, M3 (Figure 5c). Higher catalytic activity was observed for this membrane, as expected. At a pressure of 1.5 bar, this membrane showed 72% single-pass conversion of Cr(VI), which increased to 98% at a TMP of 0.5 bar. Given the very high Cr(VI) concentration in the feed, the permeate Cr(VI) concentration does not meet the World Health Organization (WHO) guideline of 50  $\mu$ g/L Cr(VI) even at this high conversion. However, the catalytic reaction is pseudo-first-order for Cr(VI) concentration as long as sufficient reducing agent is present in the system. 38,63,67 This means that the final conversion should be independent of feed concentration for the same residence time. Therefore, if the feed concentration were more in line with typical Cr(VI) concentrations in contaminated groundwater (typically lower by an order of magnitude or more), the effluent would easily

meet WHO guidelines. This high conversion also easily supersedes the 95% conversion goal set at a comprehensive pilot study led by the city of Glendale, CA, comparing different dichromate reduction technologies. In short, while these initial results are preliminary and obtained under conditions that do not necessarily reflect realistic conditions, they are highly promising for the successful use of this technology for the remediation of contaminated groundwater streams.

Importantly, the membrane showed no deterioration of catalytic activity upon 3 days of continuous operation. The conversion remains essentially constant, indicating no poisoning or leaching of Pd-TMV occurs from the membranes. The high catalytic activity and stability of hybrid membranes shown in Figure 5 further indicate the synergistic advantage of integrating Pd-TMV complexes within the hydrogel selective layer. Given the small size of the NPs, any leaching or aggregation of Pd NPs would be expected to lead to a decline in catalyst surface area and thus lower catalytic activity. Therefore, the unchanged catalytic activity of the Pd-TMV complexes embedded in membranes throughout this 3 day long continuous experiment implies the Pd NPs remain stable, with no measurable leaching or aggregation. These results support our previous studies, which document that Pd NPs supported on TMV when embedded in hydrogels are stable over extended time periods and several reaction cycles, with no measurable leaching or loss in catalytic activity. 38,63,67

Integration of Pd-TMV complexes within the hydrogel not only confers high stability but also enhances their catalytic activity, as reported earlier.<sup>38</sup> These advantages are retained when Pd-TMV complexes are integrated into a membrane using IIFRP, even when exposed to shear in flow-through mode, and in continuous operation for long time periods. In our integrated synthesis-fabrication approach, TMV templates provide abundant adsorption sites for the Pd precursors, leading to preferential formation of small and pristine Pd NPs under mild aqueous conditions and enabling high catalytic

activity. In turn, the robust structure and network formation of the TMV ensure that the small Pd NP catalysts are retained through flow conditions in the catalytic reaction environment without leaching or aggregation, while providing the reactants ample access to the catalytic sites.<sup>38</sup> The simple IIFRP approach enables the Pd-TMV complexes to be seamlessly integrated into membranes inside thin, uniform, and stable hydrogel selective layers that allow steady and long-term operations in flow-through mode with sufficient catalytic conversion in a single pass for complete remediation of toxic compounds. In short, the long-term flow operation results shown in Figure 5 clearly illustrate the stability and robustness of the hybrid membranes with sufficient catalytic activity for remediation.

Comparative Analysis of the Reaction Kinetics in Batch and Flow-Through Modes. The results obtained in the in-line filtration setup can be further utilized to calculate the rate constant for flow-through mode. We hypothesized that since flow can improve the mass transfer between the solutes and NPs, the hydrogel membrane format should provide improved conversion and a higher apparent rate constant. We considered the hydrogel layer as a plug flow reactor because the solute concentration varies as the solution proceeds within the hydrogel layer. Longer exposure to catalytic NPs leads to higher conversion. Following a pseudo-first-order reaction mechanism for catalytic reduction, the apparent rate constant in flow-through mode,  $k_{\rm m}$ , can be calculated for our hybrid membranes with swollen hydrogel layer thickness of *l* prepared at various Pd-TMV concentrations (see Table S2 and Figure S5). Figure 5d illustrates the plot for  $k_m l$  vs Pd concentration in the monomer solution used in membrane manufacture, which is expected to be proportional to the concentration of Pd NPs in the membrane. A linear correlation between the  $k_m$  and Pd concentration in aqueous monomer solution was observed. This indicates that the Pd NPs embedded in the hydrogel network are fully accessible to the reactant for the reduction reaction, with minimal apparent diffusion limitation.

An important parameter that would enable the explicit calculation of both the residence time and the rate constant  $k_{\rm m}$ is the selective layer thickness l in the wet state. Although the FESEM shows a dry hydrogel layer thickness of 120 nm, the wet thickness is expected to be significantly higher due to swelling upon contact with water during filtration. Hydrogel swelling depends on multiple parameters such as cross-link density, hydrogel chemistry, and the pH and ionic strength of the solution. 73,74 PEG-based hydrogel layers have been reported to swell up to 10 times.<sup>75</sup> Assuming this maximum swelling ratio, a wet hydrogel layer thickness of 1  $\mu$ m is a reasonable estimate. Based on this assumption, an estimated  $k_{\rm m}$ value can be calculated. For both M1 and M3 membranes, prepared at different Pd-TMV concentrations, very high  $k_{\rm m}$ values of about 40 and 120 min<sup>-1</sup> were obtained, respectively. This remarkably high value of the reaction rate constant,  $k_{\rm m}$ , in comparison to  $k_{\rm app}$  values obtained from static reaction experiments (Figure 3) signifies improvement in mass transfer of the reactants to the catalyst in flow-through mode, further improving their performance.

# CONCLUSIONS

This study demonstrates a novel and scalable synthesisfabrication approach to create catalytically active membranes by seamless integration of Pd-TMV nano-biocomplexes into uniform, ultrathin hydrogel selective layers. As the first step of this process, highly active, uniform, and small (1-2 nm) Pd NPs were synthesized exclusively on TMV nanotemplates. As the second step, a simple and highly reproducible IIFRP technique enabled seamless integration of Pd-TMV nanobiocomplexes within ultrathin, uniform, and defect-free hydrogel selective layers. Using the IIFRP method, we can readily control catalyst loading for desired catalytic activity for various applications (waste treatment before discharge vs drinking water) simply by altering the concentration in the monomer solution. Hybrid hydrogel membranes prepared by IIFRP exhibited high catalytic activity for the dichromate reduction reaction. The integration of the NPs in this membrane platform resulted in extremely high apparent rate constants due to flow-through mode operation in a membrane system that circumvents mass transfer limitations commonly observed in other systems (e.g., particles). Taken together, these results indicate that our integrated synthesis-fabrication approach using IIFRP combines the distinct features of TMV nanotemplates with seamless integration and high stability of NPs into membranes in an easily accessible hydrophilic hydrogel selective layer. This system allows very high singlepass conversions in a simple, easy-to-operate filtration system that has the potential to also remove other larger pollutants (e.g., microorganisms and some macromolecular pollutants) due to its small pore size. These results show promise for the use of the IIFRP technique to create advanced membranes with multiple functionalities that combine catalytic activity with selectivity, leading to simple, portable, easy to use, and effective systems for water decontamination. They also demonstrate the potential of the IIFRP method for creating other multifunctional membranes that integrate nanomaterials (e.g., carbon nanotubes, catalytic nanoparticles, and adsorbent particles) into thin hydrogel layers.

### EXPERIMENTAL SECTION

Materials. Poly(ethylene glycol) diacrylate (PEGDA, average  $M_n$ 700 Da), poly(ethylene glycol) (PEG, average  $M_n$  200 and  $M_n$  8000 Da), 2-hydroxy-2-methylpropiophenone also known as Darocur 1173 (photoinitiator, PI), sodium tetrachloropalladate(II), Na2PdCl4, potassium dichromate (K<sub>2</sub>Cr<sub>2</sub>O<sub>7</sub>), sulfuric acid (H<sub>2</sub>SO<sub>4</sub>, 99.9%), Lascorbic acid (>98%), sodium hydroxide (NaOH), and potassium chloride (KCl) were purchased from Sigma-Aldrich (St. Louis, MO). n-Hexadecane (99%) was purchased from ACROS Organics. Sodium formate (HCOONa, 99%), sodium phosphate monobasic anhydrous (99%), sodium phosphate dibasic anhydrous (≥99%), ethylenediaminetetraacetic acid (EDTA), disodium salt dihydrate, and D-sucrose were purchased from Fisher Scientific (Waltham, MA). 1,4-Dithio-DL-threitol (98%) was purchased from Alfa Aesar. Reagent alcohol was obtained from VWR (West Chester, PA). All the chemicals were analytical grade and used without further purification. Ultrapure deionized water generated by Biolab 3300 RO, a building wide RO/DI water purification unit by Mar Cor Purification, was used for all experiments. Polysulfone (PS35, 20 kDa) ultrafiltration membranes purchased from Nanostone Water, Inc. (Oceanside, CA), were used as the support membrane to provide mechanical stability.

Producing and Extracting Genetically Modified Tobacco Mosaic Virus (TMV1Cys). The first generation of tobacco mosaic virus (TMV1cys) genetically modified to display surface cysteines was from Dr. James Culver at the Institute of Bioscience and Biotechnology Research at University of Maryland Biotechnology Institute. The TMV1cys templates were produced by growing and infecting tobacco plants with TMV1cys and extracting them from infected tobacco leaves with phosphate extraction buffer, followed by chloroform phase separation, PEG8000 sedimentation, and sucrose gradient for TMV purification as previously described. 76,77 Briefly, 1 mg mL<sup>-1</sup> TMV1cys in 0.1 M sodium phosphate buffer (SPB) pH 7

was used to inoculate Nicotiana tabacum L. cv Xanthi, a systemic TMV host. The infected leaves were harvested 20 days postinoculation. TMV1cys were extracted from the leaves in a blender by using phosphate extraction buffer (10 mM Na<sub>2</sub>HPO<sub>4</sub>, 10 mM EDTA, 10 mg mL<sup>-1</sup> ascorbic acid, 0.5 mM 1,4-dithio-DL-threitol). The TMV1cys extract was separated from solids using cheese cloth and poured into plastic centrifuge bottles. After adding 10% v/v chloroform, the TMV extract was mixed on ice for 30 min on a rotator, added into 100 mL centrifuge bottles, and centrifuged for 10 min at 10000 rpm and 4 °C (Beckman Coulter Allegra X-15R centrifuge, FX6100 fixed angle rotor). The supernatant was collected in a 1000 mL graduated cylinder. In a beaker with a magnetic stir bar, the supernatant, 6% w/v PEG (M<sub>n</sub> 8000 Da), and 1.5% w/v KCl were stirred for 1 h at 4 °C on a magnetic stir plate, poured into plastic bottles, and centrifuged for 10 min at 10000 rpm and 4 °C to pellet the TMV1cys. The supernatant was discarded, and the pellet was further concentrated by centrifuging for 5 min at 10000 rpm and 4 °C. The TMV1cys pellets were resuspended in 0.1 M SPB pH 7 overnight at 4 °C. To purify the TMV1cys, the resuspended TMV1cys were added to 25% w/v sucrose gradients and centrifuged for 2 h at 22500 rpm and 4 °C (Beckman Coulter Optima L-90K ultracentrifuge, SW 32 TI or SW 55 Ti swinging bucket rotor). The resulting white bands of TMV1cys were collected with a 5 mL syringe into separate centrifuge tubes with 0.1 M SPB pH 7 and centrifuged for 2 h at 30000 rpm and 4 °C (Beckman Coulter Optima L-90K ultracentrifuge, Type 70 Ti fixed angle rotor). The supernatant was discarded, and the purified TMV1cys pellets were resuspended and stored in 0.1 M SPB pH 7 at 4 °C. The concentration (mg mL<sup>-1</sup>) of the TMV1cys was obtained via UV-vis at 260, 280, and 325 nm by using Beer's law accounting for light scattering, given in eq 1:

$$[TMV] = \frac{1}{\varepsilon} [A_{260} - (2.4414 \times A_{325})] \times D \tag{1}$$

and the purity of the TMV1cys was obtained in eq 2:

$$purity = \frac{A_{260}}{A_{280}} \tag{2}$$

where  $\varepsilon = 3.0 \text{ mL mg}^{-1} \text{ cm}^{-1}$  is the extinction coefficient for TMV,  $A_{260}$ ,  $A_{280}$ , and  $A_{325}$  are the absorbance at 260, 280, and 325 nm, and D is the dilution factor.

Synthesis of Pd Nanoparticles on TMV Nanotemplates and **Characterization.** To prepare the precursor solution for formation of Pd NPs on TMV, a solution containing 0.5 mL of 1.2 mg mL-TMV in sodium phosphate buffer was added to 0.5 mL of 20 mM aqueous solution of Na<sub>2</sub>PdCl<sub>4</sub>. The solution was then incubated in a heating block at 50 °C for 30 min and centrifuged at 9000g for 5 min by using a Microfuge 22R centrifuge (Beckman Coulter, Brea, CA). The supernatant was then discarded, and the collected brown Pd-TMV complex pellets were resuspended in 50  $\mu$ L of deionized water.

Formation of Pd NPs on TMV nanotemplates and NP size distribution were characterized by using a TEM (FEI Technai Spirit) operated at 80 kV. TEM samples were prepared by placing 10  $\mu$ L of well-dispersed Pd-TMV solution onto a TEM grid (CF200-Cu, Electron Microscopy Sciences, Hatfield, PA), followed by air-drying.

Fabrication of Hybrid Hydrogel-Coated Membranes by IIFRP. The support membrane (Polysulfone, PS, Nanostone) was first washed with ethanol, dried, and then taped along all edges onto a glass plate. Aqueous monomer solutions containing 5% v/v PEGDA (700 g mol<sup>-1</sup>), 2.5% v/v PEG200, and varying Pd-TMV concentrations were prepared. To make monomer solutions containing TMV with final concentration of 1, 3, and 10 mg mL<sup>-1</sup>, varying volumes (1, 3, and 10 mL) of Pd-TMV solution (0.6 mg mL<sup>-1</sup> TMV, 10 mM Na<sub>2</sub>PdCl<sub>4</sub>) were centrifuged, and the collected pellets were resuspended in 50  $\mu$ L of deionized water, mixed with PEG200 and PEGDA. The aqueous monomer solution was then poured on the support membrane. The support membrane was equilibrated with the solution for 3 min to provide enough time for monomers and porogen to diffuse into the pores. The penetration of PEGDA into PS helps further stability of the coating layer on PS. Given the large size of Pd-TMV complexes (18 nm diameter × 300

nm length,  $D_{\rm h} \sim 110$  nm), they most likely remain on the membrane surface. The aqueous solution was then poured out, and the membrane surface was gently dabbed using filter paper to remove any residual droplets. A solution of 0.1% v/v of oil-soluble PI (Darocur) in n-hexadecane (i.e., wetting fluid) was poured on the membrane surface. The membrane surface was covered with a glass plate to prevent initiation from the PS support membrane.<sup>5</sup> Subsequently, the membrane was exposed to 365 nm UV light with an 8 W hand-held UV lamp (Spectronics Corp., Westbury, NY) for 7 min. The excess solution covering the membrane was then poured out, and the membrane surface was washed with a water/ethanol mixture 2:1 ratio several times and kept in deionized water overnight to ensure the complete removal of unreacted monomer, NPs, initiator, and hexadecane.

Catalytic Activity of Hybrid Hydrogel-Coated Membranes in Static Reaction. The catalytic activity of the membranes containing various amounts of Pd-TMV complexes was tested via reduction of dichromate solution. For this, 1 mL of reaction solution containing 0.1 mM K<sub>2</sub>Cr<sub>2</sub>O<sub>7</sub> and 100 mM HCOONa (pH adjusted to 3 by adding H<sub>2</sub>SO<sub>4</sub>) was poured on the membrane surface with nearsurface stirring by magnetic stirrer at around 200 rpm. The reduction was monitored by using a UV-vis spectrophotometer (Thermo Scientific Genesys10S spectrometer, Waltham, MA) at 350 nm, the characteristic absorption peak of dichromate ions. The concentration of Cr(VI) was calculated by using a calibration curve derived from standard solution, and conversion, x, was calculated via eq 3:

$$x\% = \frac{[Cr(VI)_0] - [Cr(VI)_t]}{[Cr(VI)_0]} \times 100$$
(3)

where  $Cr(VI)_0$  is the feed concentration, 0.1 mM, and  $Cr(VI)_t$  is the concentration at each time point.

The presence of Cr(III) as the reaction product was confirmed by adding an excess of sodium hydroxide solution, where an emergence of a green color indicates the formation of hexahydroxochromate(III).

Kinetic Study of the Cr(VI) Redox Reaction. The coupled redox reactions are listed as

$$Cr_2O_7^{2-} + 14H_3O^+ + 6e^- \leftrightarrow 2Cr^{3+} + 21H_2O$$

$$\text{HCOOH} + 2\text{H}_2\text{O} \leftrightarrow \text{CO}_2 + 2\text{H}_3\text{O}^+ + 2\text{e}^-$$

Under the reaction conditions used in this study, the reduction reaction follows pseudo-first-order kinetics with respect to Cr(VI) concentration. The apparent first-order rate constant was obtained from the slope of linear regression ln(1 - x) vs time.

Catalytic Activity of Hybrid Hydrogel-Coated Membranes in Dead-End Filtration Experiments. To study the membranes catalytic activity in continuous mode, we ran filtration experiments using an Amicon 8010 dead-end stirred cell (Millipore) with a cell volume of 10 mL and an effective filtration area of 4.1 cm<sup>2</sup>, while the cell was stirring at about 500 rpm at an applied transmembrane pressure (TMP) of 1 bar. Water flow rate through the membranes was measured by collecting the permeate in a container placed on a scale (Ohaus Scout Pro) over time at TMP of 2.7 bar (40 psi). The membrane permeance  $(L_p)$  was calculated by normalizing flux (J), defined as the water flow rate divided by active membrane area, with TMP  $(\Delta P)$ :

$$L_{\rm p} = \frac{J}{\Delta P} \tag{4}$$

The membrane performance for catalytic reduction of Cr(VI) was studied by filtering a 10 mL solution containing 0.1 mM K<sub>2</sub>Cr<sub>2</sub>O<sub>7</sub> solution and 100 mM HCOONa at pH 3 (adjusted by H<sub>2</sub>SO<sub>4</sub>), i.e., reaction solution. Tests were conducted at TMP of 1 bar by continuously collecting 0.5 mL of permeate and measuring their absorbance at 350 nm. The conversions were calculated via eq 3.

Catalytic Activity of Hybrid Hydrogel-Coated Membranes in In-Line Filtration Experiments and Kinetic Studies. To study the stability of membranes' catalytic activity as well as effect of residence time, we performed long-term filtration experiments using

an in-line filter holder with effective area of 0.9 cm<sup>2</sup> (Cole-Parmer, Vernon Hills, IL) attached to a 1 gallon reservoir. The reaction solution was continuously fed to the membrane, and the permeates were collected by using a fraction collector at various TMP (0.25–1.5 bar). The conversion was calculated subsequently by using eq 3. To obtain the apparent rate constant, a mole balance was applied to the hydrogel layer, assuming that Pd–TMV NPs are well-dispersed within selective layer and considering the membrane as a plug flow reactor.

# ASSOCIATED CONTENT

# **S** Supporting Information

The Supporting Information is available free of charge on the ACS Publications website at DOI: 10.1021/acsanm.9b01099.

Additional SEM images and detailed description of the calculation of rate constants (PDF)

#### AUTHOR INFORMATION

## **Corresponding Authors**

\*(H.Y.) E-mail hyunmin.yi@tufts.edu.

\*(A.A.) E-mail ayse.asatekin@tufts.edu.

#### ORCID

Ilin Sadeghi: 0000-0002-3451-0709 Ayse Asatekin: 0000-0002-4704-1542

#### **Present Address**

I.S.: David H. Koch Institute of Integrative Cancer Research, Massachusetts Institute of Technology, 500 Main Street, Cambridge, MA 02139.

#### Notes

The authors declare no competing financial interest.

## ACKNOWLEDGMENTS

We gratefully acknowledge financial support from Tufts University, the Tufts Collaborates program, and the National Science Foundation (NSF) under Grants CBET-1703549 and CBET-1553661. TEM was performed by utilizing the W.M. Keck foundation Biological Imaging Facility at the Whitehead Institute. We thank Dr. Nicki Watson at the Whitehead Institute for help with TEM data acquisition. FESEM imaging was performed at the Center for Nanoscale Systems (CNS), a member of the National Nanotechnology Infrastructure Network (NNIN), which is supported by the National Science Foundation under NSF Award ECS-0335765. CNS is part of Harvard University.

# REFERENCES

- (1) National Research Council, Environmental Epidemiology, Public Health and Hazardous Wastes; National Academy Press: Washington, DC, 1991; Vol. 1.
- (2) Kotas, J.; Stasicka, Z. Chromium occurrence in the environment and methods of its speciation. *Environ. Pollut.* **2000**, 107 (3), 263–283
- (3) Keith, L. H.; Telliard, W. A. Priority Pollutants I-a Perspective View. *Environ. Sci. Technol.* **1979**, *13* (4), 416–423.
- (4) Guidlines for Drinking Water Quality, 2nd ed.; World Health Organization: Geneva, 1996; Vol. 2.
- (Ś) Barrera-Diaz, C. E.; Lugo-Lugo, V.; Bilyeu, B. A review of chemical, electrochemical and biological methods for aqueous Cr(VI) reduction. *J. Hazard. Mater.* **2012**, 223, 1–12.
- (6) Fu, F. L.; Wang, Q. Removal of heavy metal ions from wastewaters: A review. J. Environ. Manage. 2011, 92 (3), 407–418.
- (7) Costa, M. Toxicity and carcinogenicity of Cr(VI) in animal models and humans. Crit. Rev. Toxicol. 1997, 27 (5), 431–442.

- (8) Zhitkovich, A. Chromium in Drinking Water: Sources, Metabolism, and Cancer Risks. *Chem. Res. Toxicol.* **2011**, 24 (10), 1617–1629.
- (9) Vankelecom, I. F. J. Polymeric membranes in catalytic reactors. *Chem. Rev.* **2002**, *102* (10), *3779*–3810.
- (10) Zaman, J.; Chakma, A. Inorganic Membrane Reactors. J. Membr. Sci. 1994, 92 (1), 1–28.
- (11) Argyle, M. D.; Bartholomew, C. H. Heterogeneous Catalyst Deactivation and Regeneration: A Review. *Catalysts* **2015**, *5* (1), 145–269.
- (12) Gu, X. J.; Lu, Z. H.; Jiang, H. L.; Akita, T.; Xu, Q. Synergistic Catalysis of Metal-Organic Framework-Immobilized Au-Pd Nanoparticles in Dehydrogenation of Formic Acid for Chemical Hydrogen Storage. *J. Am. Chem. Soc.* **2011**, *133* (31), 11822–11825.
- (13) Pozniak, G.; Krajewska, B.; Trochimczuk, W. Urease Immobilized on Modified Polysulfone Membrane Preparation and Properties. *Biomaterials* **1995**, *16* (2), 129–134.
- (14) Rizvi, A.; Chu, R. K. M.; Lee, J. H.; Park, C. B. Superhydrophobic and Oleophilic Open-Cell Foams from Fibrillar Blends of Polypropylene and Polytetrafluoroethylene. *ACS Appl. Mater. Interfaces* **2014**, *6* (23), 21131–21140.
- (15) Dandapat, A.; Jana, D.; De, G. Pd nanoparticles supported mesoporous gamma-Al<sub>2</sub>O<sub>3</sub> film as a reusable catalyst for reduction of toxic  $Cr^{VI}$  to  $Cr^{III}$  in aqueous solution. *Appl. Catal., A* **2011**, 396 (1–2), 34–39.
- (16) Yadav, M.; Xu, Q. Catalytic chromium reduction using formic acid and metal nanoparticles immobilized in a metal-organic framework. *Chem. Commun.* **2013**, 49 (32), 3327–3329.
- (17) Huang, Y.; Ma, H.; Wang, S.; Shen, M.; Guo, R.; Cao, X.; Zhu, M.; Shi, X. Efficient Catalytic Reduction of Hexavalent Chromium Using Palladium Nanoparticle-Immobilized Electrospun Polymer Nanofibers. ACS Appl. Mater. Interfaces 2012, 4 (6), 3054–3061.
- (18) Uozumi, Y.; Nakao, R. Catalytic Oxidation of Alcohols in Water under Atmospheric Oxygen by Use of an Amphiphilic Resin-Dispersion of a Nanopalladium Catalyst. *Angew. Chem., Int. Ed.* **2003**, 42 (2), 194–197.
- (19) Yamada, Y. M. A.; Watanabe, T.; Ohno, A.; Uozumi, Y. Development of Polymeric Palladium-Nanoparticle Membrane-Installed Microflow Devices and their Application in Hydrodehalogenation. *ChemSusChem* **2012**, *5* (2), 293–299.
- (20) Zhao, Y.; Liu, L.; Shi, D.; Shi, X.; Shen, M. Performing a catalysis reaction on filter paper: development of a metal palladium nanoparticle-based catalyst. *Nanoscale Advances* **2019**, *1* (1), 342–346.
- (21) Rajeswari, A.; Vismaiya, S.; Pius, A. Preparation, characterization of nano ZnO-blended cellulose acetate-polyurethane membrane for photocatalytic degradation of dyes from water. *Chem. Eng. J.* **2017**, *313*, 928–937.
- (22) Meyer, D. E.; Wood, K.; Bachas, L. G.; Bhattacharyya, D. Degradation of chlorinated organics by membrane-immobilized nanosized metals. *Environ. Prog.* **2004**, 23 (3), 232–242.
- (23) Ludtke, K.; Peinemann, K. V.; Kasche, V.; Behling, R. D. Nitrate removal of drinking water by means of catalytically active membranes. *J. Membr. Sci.* **1998**, *151* (1), 3–11.
- (24) Hilke, R.; Pradeep, N.; Madhavan, P.; Vainio, U.; Behzad, A. R.; Sougrat, R.; Nunes, S. P.; Peinemann, K. V. Block Copolymer Hollow Fiber Membranes with Catalytic Activity and pH-Response. ACS Appl. Mater. Interfaces 2013, 5 (15), 7001–7006.
- (25) Xu, J.; Dozier, A.; Bhattacharyya, D. Synthesis of nanoscale bimetallic particles in polyelectrolyte membrane matrix for reductive transformation of halogenated organic compounds. *J. Nanopart. Res.* **2005**, 7 (4–5), 449–467.
- (26) Wu, Z. Y.; Lin, H. B.; Wang, Y. Z.; Yu, X. M.; Li, J. L.; Xiong, Z.; Wang, Y.; Huang, Y. J.; Chen, T.; Liu, F. Enhanced catalytic degradation of 4-NP using a superhydrophilic PVDF membrane decorated with Au nanoparticles. *RSC Adv.* **2016**, *6* (67), 62302–62309
- (27) Wang, J. Q.; Wu, Z. Y.; Li, T. T.; Ye, J. R.; Shen, L. Q.; She, Z.; Liu, F. Catalytic PVDF membrane for continuous reduction and

- separation of p-nitrophenol and methylene blue in emulsified oil solution. Chem. Eng. J. 2018, 334, 579-586.
- (28) Dotzauer, D. A.; Bhattacharjee, S.; Wen, Y.; Bruening, M. L. Nanoparticle-Containing Membranes for the Catalytic Reduction of Nitroaromatic Compounds. *Langmuir* **2009**, 25 (3), 1865–1871.
- (29) Dotzauer, D. M.; Dai, J. H.; Sun, L.; Bruening, M. L. Catalytic membranes prepared using layer-by-layer adsorption of polyelectrolyte/metal nanoparticle films in porous supports. *Nano Lett.* **2006**, 6 (10), 2268–2272.
- (30) Lewis, S. R.; Datta, S.; Gui, M. H.; Coker, E. L.; Huggins, F. E.; Daunert, S.; Bachas, L.; Bhattacharyya, D. Reactive nanostructured membranes for water purification. *Proc. Natl. Acad. Sci. U. S. A.* **2011**, 108 (21), 8577–8582.
- (31) Pan, S. L.; Li, J. S.; Noonan, O.; Fang, X. F.; Wan, G. J.; Yu, C. Z.; Wang, L. J. Dual-Functional Ultrafiltration Membrane for Simultaneous Removal of Multiple Pollutants with High Performance. *Environ. Sci. Technol.* **2017**, *51* (9), 5098–5107.
- (32) Wan, H. Y.; Briot, N. J.; Saad, A.; Ormsbee, L.; Bhattacharyya, D. Pore functionalized PVDF membranes with in-situ synthesized metal nanoparticles: Material characterization, and toxic organic degradation. *J. Membr. Sci.* **2017**, *530*, 147–157.
- (33) Zhong, Y.; Li, T. T.; Lin, H. B.; Zhang, L.; Xiong, Z.; Fang, Q. L.; Zhang, G. Y.; Liu, F. Meso-/macro-porous microspheres confining Au nanoparticles based on PDLA/PLLA stereo-complex membrane for continuous flowing catalysis and separation. *Chem. Eng. J.* **2018**, 344, 299–310.
- (34) Kim, J.; Kim, K.; Ye, H.; Lee, E.; Shin, C.; McCarty, P. L.; Bae, J. Anaerobic Fluidized Bed Membrane Bioreactor for Wastewater Treatment. *Environ. Sci. Technol.* **2011**, *45* (2), 576–581.
- (35) Santos, N. C.; Castanho, M. A. R. B. Teaching light scattering spectroscopy: The dimension and shape of tobacco mosaic virus. *Biophys. J.* **1996**, *71* (3), 1641–1650.
- (36) Lim, J. S.; Kim, S. M.; Lee, S. Y.; Stach, E. A.; Culver, J. N.; Harris, M. T. Biotemplated Aqueous-Phase Palladium Crystallization in the Absence of External Reducing Agents. *Nano Lett.* **2010**, *10* (10), 3863–3867.
- (37) Lee, S. Y.; Royston, E.; Culver, J. N.; Harris, M. T. Improved metal cluster deposition on a genetically engineered tobacco mosaic virus template. *Nanotechnology* **2005**, *16* (7), S435–S441.
- (38) Yang, C. X.; Choi, C. H.; Lee, C. S.; Yi, H. M. A Facile Synthesis-Fabrication Strategy for Integration of Catalytically Active Viral-Palladium Nanostructures into Polymeric Hydrogel Microparticles via Replica Molding. ACS Nano 2013, 7 (6), 5032–5044.
- (39) Yang, Q.; Adrus, N.; Tomicki, F.; Ulbricht, M. Composites of functional polymeric hydrogels and porous membranes. *J. Mater. Chem.* **2011**, *21* (9), 2783–2811.
- (40) Ju, H.; McCloskey, B. D.; Sagle, A. C.; Wu, Y. H.; Kusuma, V. A.; Freeman, B. D. Crosslinked poly(ethylene oxide) fouling resistant coating materials for oil/water separation. *J. Membr. Sci.* **2008**, 307 (2), 260–267.
- (41) Sadeghi, I.; Yi, H.; Asatekin, A. A Method for Manufacturing Membranes with Ultrathin Hydrogel Selective Layers for Protein Purification: Interfacially Initiated Free Radical Polymerization (IIFRP). *Chem. Mater.* **2018**, *30* (4), 1265–1276.
- (42) Le-Clech, P.; Chen, V.; Fane, T. A. G. Fouling in membrane bioreactors used in wastewater treatment. *J. Membr. Sci.* **2006**, 284 (1–2), 17–53.
- (43) Sadeghi, I.; Aroujalian, A.; Raisi, A.; Dabir, B.; Fathizadeh, M. Surface modification of polyethersulfone ultrafiltration membranes by corona air plasma for separation of oil/water emulsions. *J. Membr. Sci.* **2013**, 430, 24–36.
- (44) Sadeghi, I.; Govinna, N.; Cebe, P.; Asatekin, A. Superoleophilic, Mechanically Strong Electrospun Membranes for Fast and Efficient Gravity-Driven Oil/Water Separation. *ACS Appl. Mater. Interfaces* **2019**, *1* (4), 765–776.
- (45) Holding, S.; Sadeghi, I.; White, T.; Murray, A.; Ray, J.; Asatekin, A.; Lantagne, D. Acceptability, effectiveness, and fouling of PointOne membrane filters distributed in South Sudan. *J. Water, Sanit. Hyg. Dev.* **2019**, *9* (2), 247–257.

- (46) Abstracts of Papers of the American Chemical Society; Zalipsky, S.; Harris, J. M. Introduction to chemistry and biological applications of poly(ethylene glycol). *ACS Symp. Ser.* **1997**, *680*, 1–13
- (47) Hou, Z.; Theyssen, N.; Brinkmann, A.; Leitner, W. Biphasic aerobic oxidation of alcohols catalyzed by poly(ethylene glycol)-stabilized palladium nanoparticles in supercritical carbon dioxide. *Angew. Chem., Int. Ed.* **2005**, 44 (9), 1346–1349.
- (48) Harraz, F. A.; El-Hout, S. E.; Killa, H. M.; Ibrahim, I. A. Palladium nanoparticles stabilized by polyethylene glycol: Efficient, recyclable catalyst for hydrogenation of styrene and nitrobenzene. *J. Catal.* **2012**, *286*, 184–192.
- (49) Huang, T. S.; Wang, Y. H.; Jiang, J. Y.; Jin, Z. L. PEG-stabilized palladium nanoparticles: An efficient and recyclable catalyst for the selective hydrogenation of 1,5-cyclooctadiene in thermoregulated PEG biphase system. *Chin. Chem. Lett.* **2008**, *19* (1), 102–104.
- (50) Mohan, Y. M.; Premkumar, T.; Lee, K.; Geckeler, K. E. Fabrication of silver nanoparticles in hydrogel networks. *Macromol. Rapid Commun.* **2006**, 27 (16), 1346–1354.
- (51) Lu, Y.; Spyra, P.; Mei, Y.; Ballauff, M.; Pich, A. Composite hydrogels: Robust carriers for catalytic nanoparticles. *Macromol. Chem. Phys.* **2007**, 208 (3), 254–261.
- (52) Ekblad, T.; Bergstroem, G.; Ederth, T.; Conlan, S. L.; Mutton, R.; Clare, A. S.; Wang, S.; Liu, Y. L.; Zhao, Q.; D'Souza, F.; Donnelly, G. T.; Willemsen, P. R.; Pettitt, M. E.; Callow, M. E.; Callow, J. A.; Liedberg, B. Poly(ethylene glycol)-Containing Hydrogel Surfaces for Antifouling Applications in Marine and Freshwater Environments. *Biomacromolecules* **2008**, *9* (10), 2775–2783.
- (53) Baxamusa, S. H.; Montero, L.; Dubach, J. M.; Clark, H. A.; Borros, S.; Gleason, K. K. Protection of Sensors for Biological Applications by Photoinitiated Chemical Vapor Deposition of Hydrogel Thin Films. *Biomacromolecules* **2008**, *9* (10), 2857–2862.
- (54) Sadeghi, I.; Kaner, P.; Asatekin, A. Controlling and Expanding the Selectivity of Filtration Membranes. *Chem. Mater.* **2018**, *30*, 7328–7354.
- (55) Wang, H. F.; Kaden, W. E.; Dowler, R.; Sterrer, M.; Freund, H. J. Model oxide-supported metal catalysts comparison of ultrahigh vacuum and solution based preparation of Pd nanoparticles on a single-crystalline oxide substrate. *Phys. Chem. Chem. Phys.* **2012**, *14* (32), 11525–11533.
- (56) Yang, C.; Yi, H. Viral Templated Palladium Nanocatalysts. ChemCatChem 2015, 7 (14), 2015–2024.
- (57) Yi, H. M.; Nisar, S.; Lee, S. Y.; Powers, M. A.; Bentley, W. E.; Payne, G. F.; Ghodssi, R.; Rubloff, G. W.; Harris, M. T.; Culver, J. N. Patterned assembly of genetically modified viral nanotemplates via nucleic acid hybridization. *Nano Lett.* **2005**, *5* (10), 1931–1936.
- (58) Yamagishi, H.; Crivello, J. V.; Belfort, G. Development of a Novel Photochemical Technique for Modifying Poly(Arylsulfone) Ultrafiltration Membranes. *J. Membr. Sci.* **1995**, *105* (3), 237–247.
- (59) Fathizadeh, M.; Tien, H. N.; Khivantsev, K.; Song, Z.; Zhou, F.; Yu, M. Polyamide/nitrogen-doped graphene oxide quantum dots (N-GOQD) thin film nanocomposite reverse osmosis membranes for high flux desalination. *Desalination* **2019**, *451*, 125–132.
- (60) Kim, H. J.; Lim, M. Y.; Jung, K. H.; Kim, D. G.; Lee, J. C. High-performance reverse osmosis nanocomposite membranes containing the mixture of carbon nanotubes and graphene oxides. *J. Mater. Chem. A* **2015**, 3 (13), 6798–6809.
- (61) Huang, H.; Qu, X. Y.; Ji, X. S.; Gao, X.; Zhang, L.; Chen, H. L.; Hou, L. Acid and multivalent ion resistance of thin film nanocomposite RO membranes loaded with silicalite-1 nanozeolites. *J. Mater. Chem. A* **2013**, *1* (37), 11343–11349.
- (62) Yoffe, S.; Fiske, G.; Giordano, M.; Giordano, M.; Larson, K.; Stahl, K.; Wolf, A. T. Geography of international water conflict and cooperation: Data sets and applications. *Water Resour. Res.* **2004**, *40* (5), W05S04.
- (63) Yang, C. X.; Meldon, J. H.; Lee, B.; Yi, H. Investigation on the catalytic reduction kinetics of hexavalent chromium by viral-templated palladium nanocatalysts. *Catal. Today* **2014**, 233, 108–116.

- (64) Yang, C. X.; Yi, H. M. Viral Templated Palladium Nanocatalysts. ChemCatChem 2015, 7 (14), 2015–2024.
- (65) McGuire, M. J.; Blute, N. K.; Seidel, C.; Qin, G.; Fong, L. Pilotscale studies of Hexavalent Chromium Removal from drinking water. *J. Am. Water Works Assoc.* **2006**, *98* (2), 134–143.
- (66) Pellerin, C.; Booker, S. M. Reflections on hexavalent chromium: health hazards of an industrial heavyweight. *Environ. Health Perspect* **2000**, 108 (9), A402.
- (67) Yang, C. X.; Manocchi, A. K.; Lee, B.; Yi, H. M. Viral templated palladium nanocatalysts for dichromate reduction. *Appl. Catal., B* **2010**, 93 (3–4), 282–291.
- (68) Sadeghi, I.; Kronenberg, J.; Asatekin, A. Selective Transport through Membranes with Charged Nanochannels Formed by Scalable Self-Assembly of Random Copolymer Micelles. *ACS Nano* **2018**, *12* (1), 95–108.
- (69) Palmer, C. D.; Wittbrodt, P. R. Processes affecting the remediation of chromium-contaminated sites. *Environ. Health Perspect.* 1991, 92, 25–40.
- (70) Omole, M. A.; K'Owino, I. O.; Sadik, O. A. Palladium nanoparticles for catalytic reduction of Cr(VI) using formic acid. *Appl. Catal., B* **2007**, *76* (1), 158–167.
- (71) McLean, J. E.; McNeill, L. S.; Edwards, M. A.; Parks, J. L. Hexavalent chromium review, part 1: Health effects, regulations, and analysis. J. Am. Water Works Assoc. 2012, 104 (6), E348–E357.
- (72) Manocchi, A. K.; Horelik, N. E.; Lee, B.; Yi, H. Simple, Readily Controllable Palladium Nanoparticle Formation on Surface-Assembled Viral Nanotemplates. *Langmuir* **2010**, *26* (5), 3670–3677.
- (73) White, E. M.; Yatvin, J.; Grubbs, J. B.; Bilbrey, J. A.; Locklin, J. Advances in smart materials: Stimuli-responsive hydrogel thin films. *J. Polym. Sci., Part B: Polym. Phys.* **2013**, *51* (14), 1084–1099.
- (74) Tokarev, I.; Minko, S. Stimuli-responsive hydrogel thin films. *Soft Matter* **2009**, 5 (3), 511–524.
- (75) Cavallo, A.; Madaghiele, M.; Masullo, U.; Lionetto, M. G.; Sannino, A. Photo-crosslinked poly(ethylene glycol) diacrylate (PEGDA) hydrogels from low molecular weight prepolymer: Swelling and permeation studies. *J. Appl. Polym. Sci.* **2017**, *134* (2), 44380.
- (76) Yang, C.; Kang, E.; Yi, H. Integrated Methods to Manufacture Hydrogel Microparticles Containing Viral—Metal Nanocomplexes with High Catalytic Activity. In *Virus-Derived Nanoparticles for Advanced Technologies. Methods in Molecular Biology*; Wege, C., Lomonossoff, G., Eds.; Humana Press: New York, 2018; Vol. 1776, pp 569–578.
- (77) Gooding, G. V.; Hebert, T. T. A Simple Technique for Purification of Tobacco Mosaic Virus in Large Quantities. *Phytopathology* **1967**, *57* (11), 1285.